



HAL
open science

Couplings between dipole and quadrupole vibrations in tin isotopes

Cédric Simenel, Philippe Chomaz

► **To cite this version:**

Cédric Simenel, Philippe Chomaz. Couplings between dipole and quadrupole vibrations in tin isotopes. Physical Review C, 2009, 80 (6), pp.064309. 10.1103/PhysRevC.80.064309 . hal-00415726v2

HAL Id: hal-00415726

<https://hal.science/hal-00415726v2>

Submitted on 11 Dec 2009

HAL is a multi-disciplinary open access archive for the deposit and dissemination of scientific research documents, whether they are published or not. The documents may come from teaching and research institutions in France or abroad, or from public or private research centers.

L'archive ouverte pluridisciplinaire **HAL**, est destinée au dépôt et à la diffusion de documents scientifiques de niveau recherche, publiés ou non, émanant des établissements d'enseignement et de recherche français ou étrangers, des laboratoires publics ou privés.

Couplings between dipole and quadrupole vibrations in tin isotopes

C. Simenel

*CEA, Centre de Saclay, IRFU/Service de Physique
Nucléaire, F-91191 Gif-sur-Yvette, France.*

Ph. Chomaz

*CEA, Centre de Saclay, IRFU/Dir,
F-91191 Gif-sur-Yvette, France. and
GANIL (DSM-CEA/IN2P3-CNRS),
B.P. 55027, F-14076 Caen cedex 5, France*

(Dated: December 11, 2009)

Abstract

We study the couplings between collective vibrations such as the isovector giant dipole and isoscalar giant quadrupole resonances in tin isotopes in the framework of the time-dependent Hartree-Fock theory with a Skyrme energy density functional. These couplings are a source of anharmonicity in the multiphonon spectrum. In particular, the residual interaction is known to couple the isovector giant dipole resonance with the isoscalar giant quadrupole resonance built on top of it, inducing a nonlinear evolution of the quadrupole moment after a dipole boost. This coupling also affects the dipole motion in a nucleus with a static or dynamical deformation induced by a quadrupole constraint or boost respectively. Three methods associated with these different manifestations of the coupling are proposed to extract the corresponding matrix elements of the residual interaction. Numerical applications of the different methods to ^{132}Sn are in good agreement with each other. Finally, several tin isotopes are considered to investigate the role of isospin and mass number on this coupling. A simple $1/A$ dependence of the residual matrix elements is found with no noticeable contribution from the isospin. This result is interpreted within the Goldhaber-Teller model.

I. INTRODUCTION

A particular interest in strongly interacting systems is their ability to present disorder or chaos, and, in the same excitation energy range, well-organized motion. Atomic nuclei are known to show both behaviors [1]. In particular, they exhibit a large variety of collective vibrations, also called giant resonances (GRs), with excitation energy usually above the particle emission threshold [2]. The GRs are associated with anomalously large cross sections in some nuclear reactions.

Baldwin and Klaiber observed the isovector giant dipole resonance (GDR) in photofission of uranium nuclei [3], interpreted as a vibration of neutrons against protons [4]. This GDR was investigated with several probes [2] and was also observed on top of highly excited states, e.g., in hot nuclei [5]. The survival of ordered motion in hot nuclei, i.e., in a chaotic environment, is one of the most striking phenomena in nuclear physics. Other kinds of GR have been discovered, such as the isoscalar giant quadrupole resonance (GQR) associated with an oscillation of the shape between a prolate and an oblate deformation [6], and the isoscalar giant monopole resonance (GMR) corresponding to a breathing mode [7, 8, 9].

The GRs are usually associated with the first phonon of a small-amplitude harmonic motion. However, the proof of their vibrational nature came with the observation of their two- and three-phonon states [10, 11, 12]. Multiphonon studies also provided a good test of the harmonic picture. In particular, anharmonicity was found in an abnormally large excitation probability of these states, indicating that different phonon states couple because of the residual interaction [13, 14]. Microscopic investigations, such as the random phase approximation (RPA) together with boson mapping techniques [15] and the nonlinear response to an external field in the time-dependent Hartree-Fock (TDHF) theory [16, 17] showed, indeed, that strong couplings between GMR, GQR and GDR occur. In particular, a GMR or a GQR (resp. a GMR) can be excited on top of a GDR (resp. a GQR), leading to couplings between one- and two-phonon states. As a consequence, GRs cannot be described in a purely harmonic picture. Anharmonicities were also found to affect pygmy dipole resonances, though depending on the choice of the nuclear functional [18].

The goal of the present work is to get a deeper insight into the couplings between various GRs, which represents a first step toward understanding complexity and disorder in nuclei at high excitation energies. As an example, we focus on the coupling between isovector

dipole and isoscalar quadrupole vibrations. A clear link between the linear dipole motion on a deformed state and the quadratic response of the quadrupole moment to an external dipole excitation (investigated in Ref. [16]) is made. The TDHF theory is used to compute the residual interaction coupling the one-phonon state of the GDR to the two-phonon state with a GQR built on top of the GDR. Applications to spherical tin isotopes are performed to investigate the role of the isospin degree of freedom and of the total number of nucleons on the coupling.

We present a schematic model describing couplings between GRs and their effect on one-body observables in Sec. II. The TDHF formalism and its application to nuclear vibrations are discussed in Sec. III. Numerical details on the 3-dimensional TDHF code are also given. A detailed investigation of the couplings in ^{132}Sn is presented in Sec. IV, together with a more systematic analysis in tin isotopes. Finally, we conclude in Sec. V.

II. A SCHEMATIC MODEL FOR GR COUPLING

Let us illustrate the effect of couplings between vibrational modes within a simple schematic model introduced in Ref. [16]. We consider the Hamiltonian

$$\hat{H} = \hat{H}_0 + \hat{V} \quad (1)$$

where \hat{H}_0 corresponds to the harmonic (HF+RPA) part and the residual interaction \hat{V} couples collective modes. Eigenstates of \hat{H}_0 are one- and two-phonon states $|\nu\rangle$ and $|\nu\mu\rangle$ with eigenenergies $E_\nu = E_0 + \hbar\omega_\nu$ and $E_{\nu\mu} = E_0 + \hbar\omega_\nu + \hbar\omega_\mu$, respectively, where $\omega_{\mu,\nu}$ denote the collective frequencies and E_0 is the ground-state energy. In the following, \hbar is omitted in the notation. Only the coupling between the two states $|\nu\rangle$ and $|\nu\mu\rangle$ is considered here. The associated matrix element of the residual interaction is noted $v_\mu = \langle\nu|\hat{V}|\nu\mu\rangle$. Such couplings between one- and two-phonon states have been proven to be the most important one in nuclei [15]. Using first-order perturbation theory, the eigenvalues of \hat{H} are those of \hat{H}_0 with eigenstates

$$|\bar{\nu}\rangle \approx |\nu\rangle - \varepsilon_\mu |\nu\mu\rangle \quad (2)$$

and

$$|\bar{\nu\mu}\rangle \approx |\nu\mu\rangle + \varepsilon_\mu |\nu\rangle \quad (3)$$

where $\varepsilon_\mu = \frac{v_\mu}{\omega_\mu}$.

The couplings are expected to affect the evolutions of expectation values of one-body observables such as the multipole moments $Q_\nu(t) \equiv \langle \hat{Q}_\nu \rangle(t)$. We investigate below three different manifestations of the couplings on these evolutions. They will be used in the next section to compute v_μ from TDHF calculations in the case of coupling between giant dipole and quadrupole resonances.

A. Quadratic response

The effect of couplings in the quadratic response has been introduced in Ref. [16]. Highlights on the main steps are given here. At initial time, the ground state $|0\rangle$ of the system is excited by a boost with the one-body operator \hat{Q}_ν

$$|\Psi(0)\rangle = \exp(-ik_\nu \hat{Q}_\nu)|0\rangle. \quad (4)$$

Developing the exponential up to second order in the boost intensity k_ν and considering an evolution under the Hamiltonian defined in Eq. (1), the state at time t reads at first order in ε_μ

$$|\Psi(t)\rangle \approx \exp(-iE_0 t) \left[\left(1 - \frac{k_\nu^2 q_\nu^2}{2} \right) |0\rangle - ik_\nu q_\nu e^{-i\omega_\nu t} (|\bar{\nu}\rangle - \varepsilon_\mu e^{-i\omega_\mu t} |\bar{\nu}\mu\rangle) \right], \quad (5)$$

where $q_\nu = \langle \nu | \hat{Q}_\nu | 0 \rangle$ is the transition amplitude that we assume to be real.

The expectation value of the one-body observable used in the boost exhibits oscillations. Indeed, in case of no static deformation in the ground state, we have

$$Q_\nu(t) = -2k_\nu q_\nu^2 \sin(\omega_\nu t) + O(k_\nu^3). \quad (6)$$

In particular, its amplitude increases linearly with the boost intensity in the small amplitude regime. In addition to this linear response, the coupling induces an oscillation of the other collective mode Q_μ :

$$Q_\mu(t) \approx 2k_\nu^2 q_\nu^2 q_\mu \frac{v_\mu}{\omega_\mu} [\cos(\omega_\mu t) - 1] \quad (7)$$

where we have assumed $q_\mu = \langle \mu | \hat{Q}_\mu | 0 \rangle = \langle \mu\nu | \hat{Q}_\mu | \nu \rangle$. This oscillation is then quadratic in k_ν and provides a first method to compute the residual interaction v_μ , assuming the fact that a nonlinear theory, such as TDHF, is used to follow the expectation values of the one-body observables. We finally note that $Q_\nu(t)$ and $Q_\mu(t)$ have different frequencies and start in phase quadrature.

B. Linear response in an external static field

It is interesting to note that the coupling may also manifest itself in the linear response to the boost (4) if an external static field is added to the Hamiltonian (1)

$$\hat{H}(\lambda) = \hat{H}(0) + \lambda \hat{Q}_\mu. \quad (8)$$

We choose λ small enough to induce a linear static deformation defined as

$$Q_\mu^0(\lambda) = \langle 0(\lambda) | \hat{Q}_\mu | 0(\lambda) \rangle \approx \lambda \left(\frac{\partial Q_\mu^0}{\partial \lambda} \right)_{\lambda=0}, \quad (9)$$

where the ground state $|0(\lambda)\rangle$ of $\hat{H}(\lambda)$ contains a contribution of the one-phonon state $|\mu\rangle$:

$$|0(\lambda)\rangle \approx |0\rangle + \frac{\lambda}{2q_\mu} \left(\frac{\partial Q_\mu^0}{\partial \lambda} \right)_{\lambda=0} |\mu\rangle. \quad (10)$$

The external potential modifies linearly the eigenenergies of the Hamiltonian and the frequency of the linear response to a boost (4) on $|0(\lambda)\rangle$ follows

$$\left(\frac{\partial \omega_\nu}{\partial \lambda} \right)_{\lambda=0} = \frac{v_\mu}{q_\mu} \left(\frac{\partial Q_\mu^0}{\partial \lambda} \right)_{\lambda=0}, \quad (11)$$

providing another direct way to extract the matrix element v_μ of the residual interaction. We emphasize the fact that, here, the nonlinear response is not invoked and a RPA code allowing static deformation in the ground state would be sufficient to compute such couplings.

C. Response to two simultaneous excitations

We showed two manifestations of the coupling (*i*) in the quadratic response and (*ii*) in the linear response under a static constraint. Let us now introduce a third one where the response $Q_\nu(t)$ is studied after a simultaneous double boost of \hat{Q}_μ and \hat{Q}_ν :

$$|\Psi(0)\rangle = e^{-ik_\mu \hat{Q}_\mu} e^{-ik_\nu \hat{Q}_\nu} |0\rangle. \quad (12)$$

The \hat{Q}_μ term modifies the response of Eq. (6) with an additional term

$$\begin{aligned} \Delta Q_\nu(t) &= \langle \hat{Q}_\nu \rangle(t) - \langle \hat{Q}_\nu \rangle_{k_\mu=0}(t) \\ &= 4k_\nu k_\mu q_\nu^2 q_\mu \frac{v_\mu}{\omega_\mu} [1 - \cos(\omega_\mu t)] \cos(\omega_\nu t). \end{aligned} \quad (13)$$

It is convenient to write this evolution with the form

$$\begin{aligned} x(t) &= \frac{Q_\nu(t)}{\overline{Q}_\nu} \\ &= \sin \omega_\nu t - \beta \cos \omega_\nu t + \frac{\beta}{2} \cos(\omega_\mu + \omega_\nu)t + \frac{\beta}{2} \cos(\omega_\mu - \omega_\nu)t \end{aligned} \quad (14)$$

where $\overline{Q}_\nu = -2k_\nu q_\nu^2$ and $\beta = 2k_\mu q_\mu v_\mu / \omega_\mu$. In fact, we can show that $x(t)$ is a solution of the differential equation

$$\frac{\ddot{x}}{\omega_\nu^2} + \left[1 - 2\beta \frac{\omega_\mu}{\omega_\nu} \sin \omega_\mu t \right] x + \beta \frac{\omega_\mu^2}{\omega_\nu^3} \dot{x} \cos \omega_\mu t = 0 \quad (15)$$

if one keeps only the first-order terms in β . The two first terms of the left-hand side are equivalent to a Mathieu's equation. It is not surprising because the latter has been shown to qualitatively reproduce the preequilibrium dipole motion coupled to collective shape vibrations of the system in N/Z asymmetric fusions [19, 20].

We see in Eq. (14) that the effect of the coupling produces vibrations at frequencies $|\omega_\nu \pm \omega_\mu|$. By analogy to the standard response function related to the strength distribution [21] we introduce the coupling response function

$$R_\nu^c(\omega) = \frac{-1}{\pi k_\nu k_\mu} \int_0^\infty dt \cos(\omega t) \Delta Q_\nu(t) \quad (16)$$

defined for $\omega \geq 0$. The latter can be used to investigate the coupling because it is linearly proportional to v_μ :

$$R_\nu^c(\omega) \approx \frac{q_\nu^2 q_\mu v_\mu}{\omega_\mu} [-2\delta(\omega_\nu - \omega) + \delta(\omega_\nu + \omega_\mu - \omega) + \delta(|\omega_\nu - \omega_\mu| - \omega)]. \quad (17)$$

Equation (17) provides then a third way to extract v_μ .

Let us finally note that the contribution to the coupling response function at ω_ν and those at $|\omega_\nu \pm \omega_\mu|$ have opposite signs in Eq. (17) and that the integral of the coupling response function is zero. It is interesting to note that this property is still valid at all order in k_ν and k_μ . To show it, let us recall that, in our schematic model, $\hat{Q}_\nu|0\rangle = q_\nu|\nu\rangle$ and $\hat{Q}_\nu^2|0\rangle = q_\nu^2|0\rangle$, which implies $e^{-ik_\nu \hat{Q}_\nu}|0\rangle = c_\nu|0\rangle - is_\nu|\nu\rangle$, where $c_\nu = \cos(k_\nu q_\nu)$ and $s_\nu = \sin(k_\nu q_\nu)$. The response $Q_\nu(t)$ following the double boost of Eq. (12) then becomes

$$Q_\nu(t) = -2c_\nu s_\nu q_\nu \sin(\omega_\nu t) + 4c_\nu c_\mu s_\nu s_\mu q_\nu \frac{v_\mu}{\omega_\mu} [1 - \cos(\omega_\mu t)] \cos(\omega_\nu t). \quad (18)$$

We see that Eq. (14) is still valid if one replaces \overline{Q}_ν by $\overline{Q}'_\nu = -2c_\nu s_\nu q_\nu$ and β by $\beta' = 2c_\mu s_\mu v_\mu / \omega_\mu$. Then, the ω -dependance of Eq. (17) is unchanged. As a consequence, the cancellation of the integral of the coupling response function defined in Eq. (16) is not limited to the small-amplitude regime.

III. THE TIME-DEPENDENT HARTREE-FOCK APPROACH

A. Applications to nuclear vibrations

Coherent motion of fermions such as collective vibrations in nuclei can be modeled by time-dependent mean-field approaches like the TDHF theory proposed by Dirac [22]. Indeed, in its linearized version, TDHF is equivalent to the RPA which is the basic tool to understand the collective vibrations in terms of independent phonons.

As we saw in the previous section, giant resonance properties can be investigated by studying the response of the system to an external (collective) one-body field. In particular, time evolution of one-body (collective) observables, which can be computed using mean-field approximations, contain the necessary information to investigate the couplings between collective modes. Indeed, TDHF takes into account the effects of the residual interaction if the considered phenomenon can be observed in the time evolution of a one-body observable. In particular, the nonlinear response in TDHF contains the couplings between one- and two-phonon states coming from the 3-particle 1-hole and 1-particle 3-hole residual interaction [16]. In that sense, it goes beyond the RPA, which is a harmonic picture and contains only 1-particle 1-hole residual interaction.

In its unrestricted form (i.e., with no constraint on spatial symmetry), TDHF authorizes all possible spatial forms of the nucleon wave functions, which is crucial because of both shell the effects and the wave dynamics. In addition, Landau spreading and evaporation damping are well accounted for [23]. However, it does not incorporate the dissipation from two-body mechanisms [24, 25, 26]. Inclusion of pairing correlations is possible within the time-dependent Hartree-Fock-Bogolyubov theory [27], but realistic applications in three dimensions are not yet achieved. Extension to theories going beyond the one-body limit such as extended TDHF [26], second RPA [28, 29], time-dependent density matrix theory [30, 31, 32] or stochastic one-body transport theory [33] should be considered for realistic description of giant resonance properties [34].

Application of TDHF to nuclear dynamics has been possible thanks to the Skyrme-type effective interaction [35, 36]. Early realistic TDHF codes have been applied to study collective vibrations in nuclei with simplified Skyrme interactions [37]. Recent increase of computational power allowed realistic TDHF description of giant resonances in 3 dimensions

with full Skyrme energy density functional (EDF) [16, 38, 39, 40, 41]. In particular, TDHF has been used to investigate nonlinear effects in nuclear vibrations [16, 42].

B. Formalism

The TDHF equation can be written as a Liouville-Von Neumann equation

$$i\frac{\partial}{\partial t}\rho = [h[\rho], \rho], \quad (19)$$

where ρ is the one-body density matrix of an independent particles state with elements

$$\rho(\mathbf{r}sq, \mathbf{r}'s'q') = \sum_{i=1}^A \varphi_i(\mathbf{r}sq)\varphi_i^*(\mathbf{r}'s'q'), \quad (20)$$

where A is the number of nucleons. The sum runs over all occupied single-particle wave functions φ_i and \mathbf{r} , s , and q denote the nucleon position, spin, and isospin respectively. The Hartree-Fock single-particle Hamiltonian $h[\rho]$ is related to the EDF, denoted by $E[\rho]$, through

$$h[\rho](\mathbf{r}sq, \mathbf{r}'s'q') = \frac{\delta E[\rho]}{\delta \rho(\mathbf{r}'s'q', \mathbf{r}sq)}. \quad (21)$$

C. Numerical details

In this work, the TDHF equation (19) is solved iteratively in time on a spatial grid with a plane of symmetry using the TDHF3D code built by P. Bonche and coworkers [43] with the SLy4 parametrization of the Skyrme EDF [44]. The latter has been constrained on the pure neutron matter equation of state to improve the description of exotic nuclei. For instance, together with a density-dependent zero-range pairing interaction, it allows a somewhat good reproduction of the isotopic shifts between proton and neutron mean-square radii in lead isotopes. It also improves the description of the isotopic evolution of the binding energies [44]. Defining the neutron drip line as the isotope for which the chemical potential vanishes, it is estimated to be around ^{176}Sn in the tin isotopic chain [45], though it might depend on the choice of the pairing interaction and on the inclusion of beyond mean-field correlations.

Good convergences of the quadrupole and dipole moment evolution is ensured with a lattice spacing $\Delta r = 0.6$ fm and a time step $\Delta t = 5 \times 10^{-25}$ s. The size of the half-box

where the single particle wave functions are evolved is $80 \times 80 \times 40$ in mesh size unit Δr , unless otherwise specified.

IV. RESULTS

Let us now investigate the coupling between isovector dipole and isoscalar quadrupole vibrations in tin isotopes in the framework of the theoretical model presented in Sec. II where $|\nu\rangle \equiv |D\rangle$ and $|\mu\rangle \equiv |Q\rangle$ denote a GDR and a GQR phonon respectively. The isovector dipole moment is defined as

$$\hat{Q}_D = \frac{NZ}{A}(\hat{Z}_n - \hat{Z}_p) \quad (22)$$

where \hat{Z}_n (resp. \hat{Z}_p) measures the neutron (resp. proton) average position on the z axis. The isoscalar quadrupole moment reads

$$\hat{Q}_Q = \sqrt{\frac{5}{16\pi}} \sum_{i=1}^A (2\hat{z}_i^2 - \hat{x}_i^2 - \hat{y}_i^2). \quad (23)$$

Their expectation value evolutions are computed using the TDHF3D code after different initial conditions as described below.

A. Nonlinear quadrupole motion induced by a dipole boost

We first investigate the quadratic response presented in Sec. II A in the ^{132}Sn nucleus. Figure 1(a) shows the early time evolution of the dipole moment after a dipole boost according to Eq. (4) in the small-amplitude regime. The dipole moment follows a $-\sin$ function as indicated by Eq. (6). Extracting the frequency from the first minimum of $D(t)$ leads to a GDR energy of $\omega_D \approx 15.2$ MeV. This value is slightly lower than the maximum of the experimental GDR peak energy $E_{max} = 16.1(7)$ MeV [46]. The same analysis in ^{120}Sn , in which almost all the dipole strength is located around the GDR energy, gives a value of $\omega_D^{(120\text{Sn})} \approx 15.3$ MeV which is in good agreement with experimental data where a peak energy of $E_{GDR}^{exp.} = 15.4$ MeV has been obtained [47]. Note that, the extraction method of ω_ν from the first extremum of $Q_\nu(t)$ is, in first approximation, comparable to the ratio of the second over the first energy weighted moments of the strength function m_2/m_1 [16].

We see in figure 1(b) that an oscillation of the quadrupole moment is induced by the dipole boost. According to the theoretical model presented in Sec. II, this is a manifestation of the

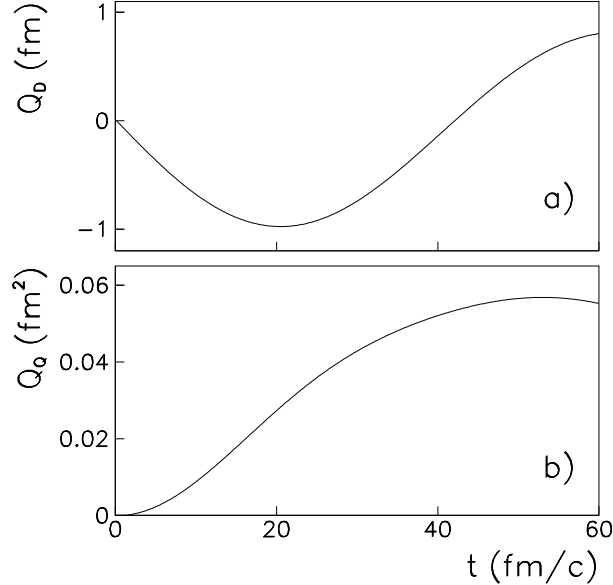


FIG. 1: Time evolution of the dipole (a) and quadrupole (b) moments in ^{132}Sn after a dipole boost with an intensity $k_D = 0.01 \text{ fm}^{-1}$.

residual interaction of Eq. (1) coupling the dipole and quadrupole vibrations. In particular, $Q_Q(t)$ starts in phase quadrature with $Q_D(t)$ and oscillates with a smaller frequency. These observations are in qualitative agreement with the quadratic response in Eq. (7).

To get a deeper insight into this coupling, we have computed the TDHF response for several dipole boost velocities k_D . The first extrema of the dipole and quadrupole moments are reported in figure 2(a) and (b) respectively. Whereas the dipole amplitude is indeed linear in k_D as expected from equation (6), indicating that these calculations are performed in the small-amplitude regime, the induced quadrupole motion is quadratic in k_D , in agreement with Eq. (7).

To obtain a quantitative estimate of the coupling, we first extract the transition amplitude from a linear extrapolation of Q_D^{min} at $k_D \rightarrow 0$ in Fig. 2(a). According to Eq. (6), we get $q_D \approx 6.98 \text{ fm}$. The same analysis with a quadrupole boost in the linear regime gives a transition amplitude $q_Q \approx 61.4 \text{ fm}^2$ and a GQR energy of $\omega_Q \approx 13.0 \text{ MeV}$. Note that the same analysis in ^{120}Sn gives a GQR energy of $\omega_Q^{(120\text{Sn})} \approx 13.3 \text{ MeV}$, in excellent agreement with the experimental value $E_{GQR}^{exp.} = 13.24 \pm 0.13 \text{ MeV}$ [48]. These quantities, together with a quadratic extrapolation of the quadrupole maximum at $k_D \rightarrow 0$ in Fig. 2(b), give, according to Eq. (7), a matrix element of the residual interaction $v_Q^{(1)} \approx -0.61 \text{ MeV}$.

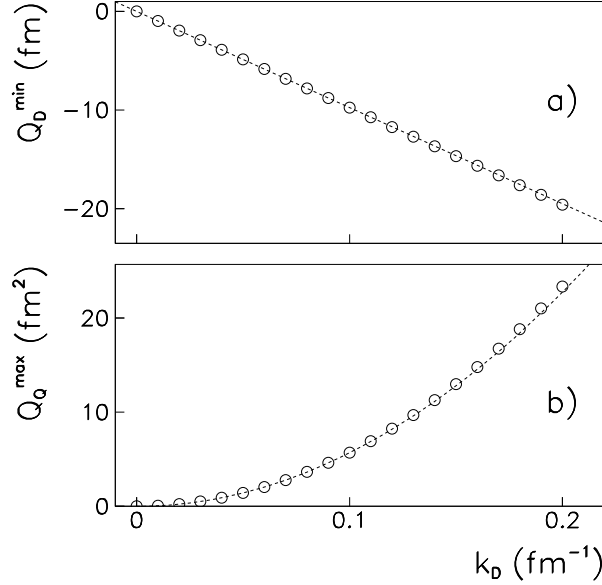


FIG. 2: Circles: First minimum and maximum of the dipole (a) and quadrupole (b) moment evolution, respectively, in ^{132}Sn as a function of the dipole boost intensity k_D . Dashed lines: linear and quadratic extrapolations at $k_D \rightarrow 0$ of the dipole (a) and quadrupole (b) amplitudes, respectively.

B. Dipole motion in a nucleus with a static quadrupole constraint

The formalism developed in Sec. II B, where the linear response is investigated in an external potential, cannot be directly applied to study the coupling between the dipole and quadrupole modes. The reason is that the external potential $-\lambda\hat{Q}_Q$ with the definition of Eq. (23) is not bound from below and its use in constrained HF calculations would lead to unphysical results. It is then necessary to consider another external potential such as

$$\lambda(\hat{Q}_Q + \kappa_\lambda \hat{Q}_M) \quad (24)$$

where

$$\hat{Q}_M = \frac{1}{\sqrt{4\pi}} \sum_{i=1}^A \hat{\mathbf{r}}_i^2 \quad (25)$$

is the monopole moment and $\kappa_\lambda = \sqrt{5}/2$ if $\lambda \geq 0$ and $-\sqrt{5}$ if $\lambda < 0$. The expression (24) then reads

$$3\sqrt{\frac{5}{16\pi}} \lambda \sum_{i=1}^A \begin{cases} \hat{z}_i^2 & \text{if } \lambda \geq 0, \\ -\hat{x}_i^2 - \hat{y}_i^2 & \text{if } \lambda < 0. \end{cases} \quad (26)$$

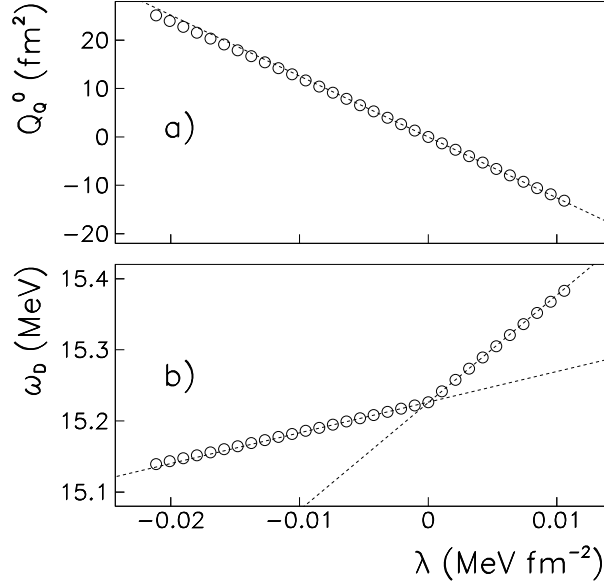


FIG. 3: (a) Static quadrupole moment from HF calculation (circles) under a quadrupole+monopole constraint (see text) as a function of the Lagrange parameter λ in ^{132}Sn . (b) TDHF energy of the GDR (circles) from the first minimum of the dipole moment after a dipole boost along the deformation axis with an intensity $k_D = 0.01 \text{ fm}^{-1}$. Dashed lines : linear extrapolations at $\lambda \rightarrow 0^\pm$ of the quadrupole moment (a) and GDR energy (b).

Such an external field allows one to explore all quadrupole deformations from oblate ($\lambda > 0$) to prolate ($\lambda < 0$) shapes as shown in figure 3(a) where the ground state quadrupole deformation Q_Q^0 of the constrained HF solution is plotted as a function of the Lagrange parameter λ . The quadrupole deformation is clearly linear in this perturbative regime and its slope at the origin is $\left. \frac{\partial Q_Q^0}{\partial \lambda} \right|_{\lambda=0} \approx -1260.4 \text{ fm}^4 \text{ MeV}^{-1}$.

As discussed in Sec. II B, such a static deformation is expected to change the dipole frequency as compared to that of the GDR excited on the spherical ground state. In fact, the frequency of a dipole oscillation along the main quadrupole axis decreases (resp. increases) with a prolate (resp. oblate) deformation. This is indeed what we observe in figure 3(b) where the energy of the GDR is plotted as a function of λ . Note that, according to Eq. (11), this is consistent with the negative sign of the ratio v_Q/q_Q obtained in Sec. IV A.

We also observe in Fig. 3(b) that the evolution of this energy is linear both for $\lambda > 0$ and $\lambda < 0$, but the slopes are different in these two regimes. This is attributed to the presence of the monopole moment in the constraint (24). Indeed, the monopole vibration is also coupled

to the dipole mode by a matrix element v_M of the residual interaction [15, 16]. According to Eq. (11), the dipole energy is expected to be modified as

$$\omega_D(\lambda) \approx \omega_D(0) + \lambda \frac{v_Q}{q_Q} \left(\frac{\partial Q_Q^0}{\partial \lambda} \right)_{\lambda=0} + \lambda \kappa_\lambda \frac{v_M}{q_M} \left(\frac{\partial Q_M^0}{\partial \lambda} \right)_{\lambda=0}. \quad (27)$$

A compression of the nucleus increases the dipole frequency, which implies $v_M/q_M < 0$. Because $\lambda \kappa_\lambda \geq 0$ for all λ , the monopole and quadrupole moments have an opposite effect on ω_D for $\lambda < 0$ and act in the same direction for $\lambda > 0$. This is indeed what we observe in Fig. 3(b) where the effect of the constraint almost cancels on the prolate side, whereas it strongly increases the GDR energy in the oblate one.

Finally, starting from Eq. (27), it is possible to isolate the coupling matrix element between the dipole and quadrupole modes

$$v_Q = \left(\frac{\partial Q_Q^0}{\partial \lambda} \right)_{\lambda=0}^{-1} \frac{q_Q}{3} \left[\left(\frac{\partial \omega_D}{\partial \lambda} \right)_{\lambda \rightarrow 0^-} + 2 \left(\frac{\partial \omega_D}{\partial \lambda} \right)_{\lambda \rightarrow 0^+} \right]. \quad (28)$$

Using the data extracted from Fig. 3 and the value of q_Q obtained in Sec. IV A, we get $v_Q^{(2)} \approx -0.56$ MeV. This result is in reasonable agreement with the one obtained with the quadratic response.

C. Response to a dipole+quadrupole boost

A third manifestation of the coupling between dipole and quadrupole motions occurs when both a dipole and a quadrupole boost are performed at initial time. We showed in Sec. II C that, in such a case, the dipole motion is affected by the quadrupole vibration. Such effect is not present in the linear response theory because the modifications are proportional to $k_D k_Q$. As can be seen in Eq. (6), there is no other quadratic term because the next-order terms affecting the dipole motion are in k_D^3 and k_Q^3 .

The basic tool to study the effect of the coupling on the dipole motion is the coupling response function defined in Eq. (16). In principle, its calculation implies to follow the dipole moment over an infinite time. However, we use a filtering procedure to avoid numerical artifacts coming from the interaction of the nucleus with reflected nucleon wave functions because of the hard box boundary conditions [49]. We perform the calculations over 3000 iterations in time (450 fm/c). The dipole moment is multiplied by a filtering function $\exp \left[-\frac{1}{2} \left(\frac{t}{\tau} \right)^2 \right]$ with $\tau = 100$ fm/c [39]. This procedure induces an additional width of

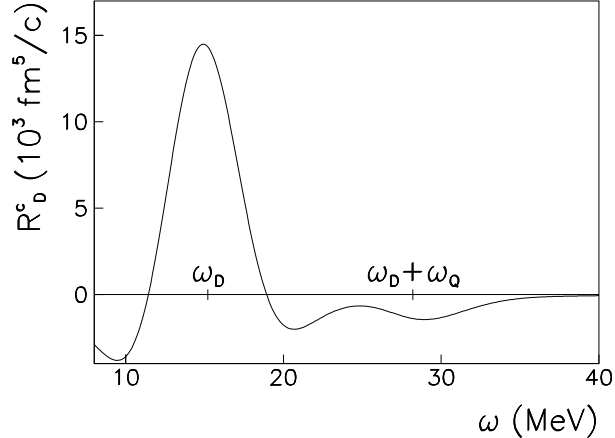


FIG. 4: Coupling response function of the dipole moment after a dipole+quadrupole boost with intensities $k_D = 0.01 \text{ fm}^{-1}$ and $k_Q = 0.001 \text{ fm}^{-2}$ respectively.

$\tau^{-1} \approx 2 \text{ MeV}$. According to Eq. (17), this additional width is sufficiently small for the present discussion because the modes in the coupling response function are located at $\omega_D - \omega_Q \approx 2.2$, $\omega_D \approx 15.2$, and $\omega_D + \omega_Q \approx 28.2 \text{ MeV}$. However, the low-energy part of the spectrum, i.e., in the region of the $\omega_D - \omega_Q$ peak, is dependent on the choice of the filtering function within these numerical conditions. We checked with other filtering functions, e.g., a cosine instead of a Gaussian function, to confirm that the higher part of the spectrum (above $\approx 10 \text{ MeV}$) is not affected. In addition, the filtering function does not change the fact that the total integral of the coupling response function vanishes (see Sec. II C). The latter was found to be a solid numerical property of this function. Finally, we checked the convergence of the results presented in this section by comparing with calculations performed in a bigger box of $120 \times 120 \times 60$ in mesh size unit Δr .

Figure 4 shows the coupling response function for the dipole motion following a quadrupole+dipole boost. We checked that, in the small-amplitude limit, the coupling response function is indeed independent of k_Q and k_D . As expected from Eq. (17), two peaks are present in this energy range at ω_D and $\omega_D + \omega_Q$ with opposite signs. Moreover, the integral of the positive peak at ω_D is directly related to the coupling as

$$v_Q = -\frac{\omega_Q}{2q_D^2 q_Q} \int_{R_D^c > 0} d\omega R_D^c(\omega). \quad (29)$$

With the coefficients calculated in Sec. IV A, we obtain a coupling $v^{(3)} \approx -0.68 \text{ MeV}$ of the same order of magnitude than with the two previous methods.

Let us finally note that in the case of more complicated vibrations, e.g., the oscillations exhibit several frequencies, the coupling response function can be used for a more detailed investigation of the coupling. Indeed, it allows an analysis of the coupling effect at each energy whereas the two previous methods give only access to a weighted sum of the matrix elements of the residual interaction associated to each excited mode [16].

D. Evolution of the coupling with isospin and mass

We now repeat the study of the linear quadrupole motion induced by a dipole boost, described in Sec. IV A, to the tin isotopic chain. The choice of this method to investigate more systematically the coupling between dipole and quadrupole vibrations is motivated by its rather low computational time as compared to the two other methods. Our goal is to understand the evolution of v_Q as a function of the isospin. To avoid any ambiguity coming from possible static deformation in the ground states, we focus on some of the tin isotopes that are spherical at the HF level: $^{100,106,114,120,132,140}\text{Sn}$. These isotopes allow for an investigation of the coupling from the proton-rich to the neutron-rich side.

Let us first investigate the linear response to a quadrupole boost (Eq. (4)) to compute the energies ω_Q and transition amplitudes q_Q from the first minimum of the quadrupole moment (see Eq. (6)). These quantities are plotted in Fig. 5 as a function of the number of nucleons. The GQR energy is known to be proportional to $A^{-1/3}$ [2]. This is compatible with the TDHF results that are fitted by $\omega_Q \approx 65.5A^{-1/3}$ MeV. The evolution of the transition amplitude with A can be obtained from the energy weighted sum rule (EWSR) for quadrupole vibrations which reads [21]

$$\begin{aligned} S_Q^1 &= \sum_{\alpha} (E_{\alpha} - E_0) |\langle \alpha | \hat{Q}_Q | 0 \rangle|^2 \\ &= \frac{\hbar^2}{m} \frac{5}{4\pi} A \langle \hat{\mathbf{r}}^2 \rangle \\ &\approx 14.3 A^{5/3} \text{ MeV} \cdot \text{fm}^4 \end{aligned} \tag{30}$$

where $\{|\alpha\rangle\}$ is an eigenbasis of \hat{H} . In the last line of Eq. 30, we used the approximation of a constant density and a sharp surface which gives $\langle \hat{\mathbf{r}}^L \rangle = \frac{3}{L+3} R^L$ with $R \approx 1.2A^{1/3}$ fm. If all the strength is located at the GQR energy, which is a somewhat good approximation for

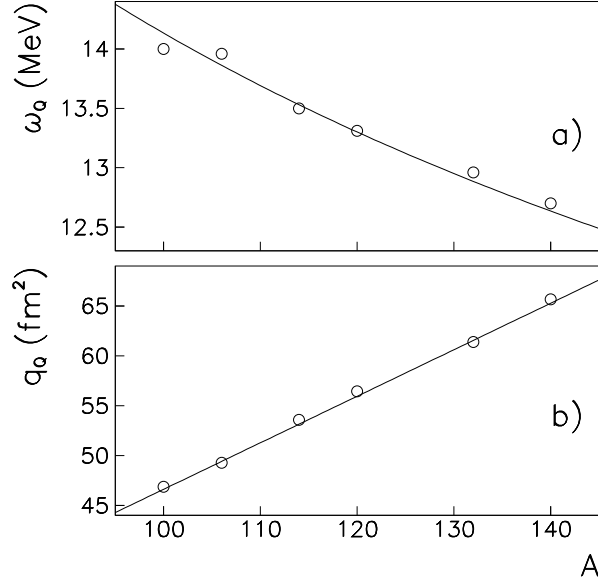


FIG. 5: Evolution of (a) the GQR energy and (b) the transition amplitude as a function of the number of nucleons in tin isotopes from the TDHF linear response (circles). The line in panel (a) represents a $A^{-1/3}$ fit of the TDHF results, whereas the line in panel (b) is obtained from considerations on the GQR energy weighted sum rule (see text).

heavy nuclei [2], then the EWSR reduces to

$$S_Q^1 = \omega_Q q_Q^2 \approx 65.5 A^{-1/3} q_Q^2. \quad (31)$$

Equations (30) and (31) then lead to

$$q_Q \approx 0.466 A \text{ fm}^2. \quad (32)$$

This linear dependence is plotted in Fig. 5(b) and reproduces well the TDHF results.

Let us now consider a dipole boost on these nuclei with a boost velocity $k_D = 0.01 \text{ fm}^{-1}$. This value is small enough to generate a linear response of the dipole moment and a quadratic response of the induced quadrupole vibration in all considered isotopes. The GDR energy ω_D is shown as a function of the number of nucleons in Fig. 6(a). It is compatible with the $A^{-1/3}$ dependence expected in heavy nuclei [2]. A fit of the TDHF results gives

$$\omega_D \approx 76 A^{-1/3} \text{ MeV}. \quad (33)$$

Similarly to the quadrupole case, the dependence of the transition probability q_D^2 can be

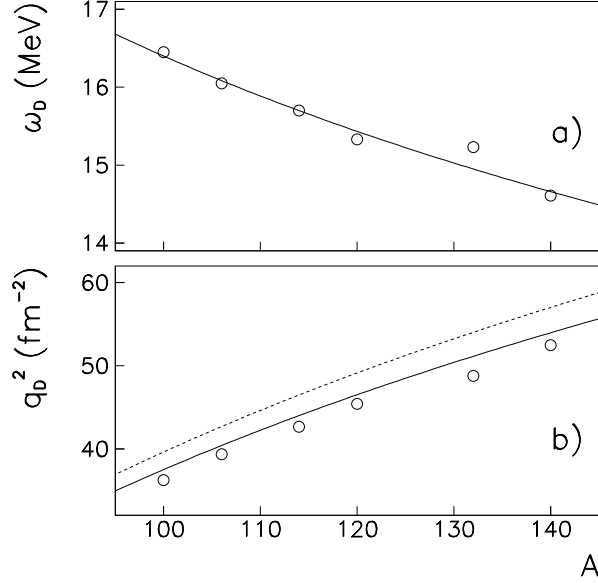


FIG. 6: Evolution of (a) the GDR energy and (b) the transition probability as a function of the number of nucleons in tin isotopes from TDHF linear response (circles). The line in panel (a) represents a $A^{-1/3}$ fit of the TDHF results. The lines in panel (b) is obtained from considerations on the GDR energy weighted sum rule (see text) with an enhancement factor of the Thomas-Reiche-Kuhn sum rule $\kappa = 0.25$ (dashed line) and $\kappa = 0.183$ (solid line).

obtained from the dipole EWSR

$$S_D^1 = \frac{\hbar^2}{2m}(1 + \kappa)\frac{NZ}{A} \quad (34)$$

where κ is the enhancement factor of the Thomas-Reiche-Kuhn (TKR) sum rule. Assuming all the strength in the GDR, i.e., $q_D^2 = S_D^1/\omega_D$, we get from Eqs. (33) and (34)

$$q_D^2 \approx \frac{\hbar^2}{2m}(1 + \kappa)\frac{NZ}{76A^{2/3}} \quad (35)$$

In nuclear matter, the enhancement factor of the TKR sum rule is $\kappa = 0.25$ with the SLy4 parametrization [44]. This value clearly overestimates the transition probabilities (see dashed line in Fig. 6(b)), though the qualitative trend is in good agreement with the TDHF results. It is possible to compute κ in finite nuclei using [50]

$$\kappa = \frac{m}{4\hbar^2} \frac{A}{NZ} [t_1(2 + x_1) + t_2(2 + x_2)] \int dr^3 \rho_n(\mathbf{r})\rho_p(\mathbf{r}) \quad (36)$$

where the t_i and x_i are the usual Skyrme parameters. In the considered tin isotopes, κ is almost constant within the range 0.181–0.186 with no particular isospin or mass dependence.

This leads to a better agreement with the transition probabilities obtained with TDHF (see solid line in Fig. 6(b)), though a slight overestimation remains. The latter could be attributed to the fragmentation of the isovector dipole response. In this case, the dipole response reads

$$Q_D(t) = -2k_D \sum_i q_{D_i}^2 \sin[(\omega_D + \delta\omega_i)t]. \quad (37)$$

In our calculations, the GDR properties (ω_D and q_D) are extracted from the first minimum of the dipole response, which obeys to

$$\frac{Q_D^{min}}{-2k_D} = \sum_i q_{D_i}^2 \cos\left(\frac{\pi \delta\omega_i}{2 \omega_D}\right) \equiv q_D^2 \leq \sum_i q_{D_i}^2. \quad (38)$$

The last inequality implies that the TKR sum rule allows one only to compute the upper limit of q_D^2 in our model.

Finally, we investigate the coupling between the quadrupole and dipole vibrations from the quadratic response. We have shown in Sec. II A that, in the presence of a nonzero matrix element v_Q of the residual interaction coupling the state $|D\rangle$ to the state $|DQ\rangle$, a dipole boost is expected to generate an oscillation of the quadrupole moment. Before studying the evolution of v_Q along the tin isotopic chain, it is mandatory to get a deeper insight into the mechanism responsible for this induced quadrupole excitation.

In a macroscopic approach, the isovector GDR is interpreted by a combination of the Steinwedel-Jensen model in which the total density is kept unchanged [51] and the Goldhaber-Teller model where proton and neutron fluids are incompressible [4]. It is obvious that the Steinwedel-Jensen model does not affect the quadrupole moment because any modification of the density of one isospin specie is exactly compensated by the other in every point of space. In the Goldhaber-Teller model, however, a displacement of the proton and neutron spheres in the opposite direction is considered. It produces a dipole moment $Q_D = \frac{NZ}{A}X$ where X is the distance between their centers. This displacement also induces a prolate shape with a quadrupole moment quadratic in X . Indeed, assuming a displacement of a proton (resp. neutron) homogeneous sphere of density $Z\rho_0/A$ (resp. $N\rho_0/A$) by $X_p = -XN/A$ (resp. $X_n = XZ/A$) produces a quadrupole moment

$$Q_Q \propto ZX_p^2 + NX_n^2 = \frac{NZ}{A}X^2. \quad (39)$$

Using Eqs.(6) and (35), one gets $Q_Q \propto NZ/A^{1/3}$.

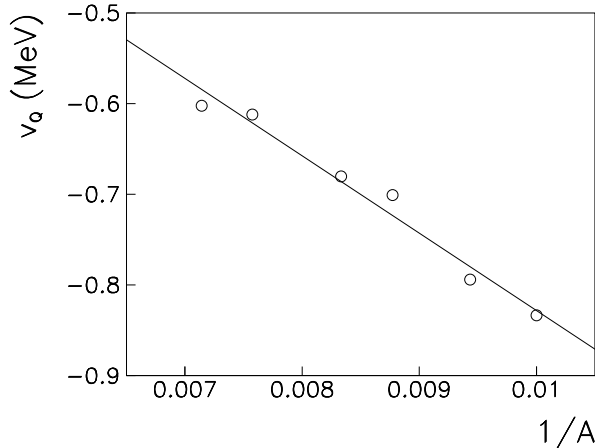


FIG. 7: Evolution of the coupling with mass number. The matrix element of the residual interaction is plotted as a function of $1/A$. The line shows a linear fit of the TDHF results.

Finally, together with Eqs. (7), (32) and (35), the evolution of the coupling simply reads $v_Q \propto 1/A$. This is, indeed, in agreement with the TDHF results shown in Fig. 7. It is interesting to note that, in this simple approach, the coupling does not depend on the isospin of the nuclei, but only on their total number of nucleons. In fact, the decrease of the absolute strength of the coupling with the number of nucleons is attributed to the fact that these couplings are mediated by the surface [16]. One then expects less anharmonicities in heavy nuclei.

V. CONCLUSIONS

We have shown that the residual interaction is responsible for anharmonicities in nuclear vibrations using three different analyses of time evolutions of multipole moments. We investigated the coupling between one- and two-phonon states using a 3-dimensional TDHF code with a full Skyrme energy density functional. In particular, the excitation of a GDR couples to a GQR built on top of it, inducing a quadratic response of the quadrupole moment. The same coupling is responsible for the change of the GDR energy in static deformed states. The latter could be investigated using deformed RPA codes. As a consequence, the dipole frequency is modulated in case of dynamical deformation, e.g., induced by a quadrupole boost. This last property, associated with a Fourier analysis, might be used to investigate couplings when more than one mode is excited with the same quantum numbers. We finally

investigated these couplings with the quadratic response in several spherical tin isotopes. As a result, no dependence with isospin was found whereas an overall decrease of the coupling is obtained with increasing mass, showing that the couplings are mediated by the surface. These observations are interpreted within the Goldhaber-Teller macroscopic model. These results indicate that no anharmonicity enhancement is expected in the standard giant resonances even for very exotic nuclei. However, couplings with exotic modes such as the pygmy dipole resonance should be investigated with the present method. The role of pairing and static deformation should be considered as well.

Acknowledgments

We thank P. Bonche for providing his TDHF code. We are also grateful to B. Avez and D. Lacroix for discussions and a careful reading of the article. Useful discussions with K. Bennaceur are also acknowledged. The calculations were performed at the Centre de Calcul Recherche et Technologie of the Commissariat à l'Énergie Atomique.

-
- [1] A. Bohr and B. Mottelson, *Nuclear Structure* (2 vol., W.A. Benjamin, Inc., New York, 1975), Vol. 2.
 - [2] M. N. Harakeh and A. van der Woude, *Giant Resonances: Fundamental High-Frequency Modes of Nuclear Excitations* (Oxford University Press, New York, 2001).
 - [3] G. C. Baldwin and G. S. Klaiber, *Phys. Rev.* **71**, 3 (1947).
 - [4] M. Goldhaber and E. Teller, *Phys. Rev.* **74**, 1046 (1948).
 - [5] J. O. Newton, B. Herskind, R. M. Diamond, E. L. Dines, J. E. Draper, K. H. Lindenberg, C. Schück, S. Shih, and F. S. Stephens, *Phys. Rev. Lett.* **46**, 1383 (1981).
 - [6] S. Fukuda and Y. Torizuka, *Phys. Rev. Lett.* **29**, 1109 (1972).
 - [7] N. Marty, A. Willis, V. Comparat, R. Frascaria, and M. Morlet, Orsay Report No. IPNO76-03, 1976.
 - [8] M. N. Harakeh, K. van der Borg, T. Ishimatsu, H. P. Morsch, A. van der Woude, and F. E. Bertrand, *Phys. Rev. Lett.* **38**, 676 (1977).
 - [9] D. H. Youngblood, C. M. Rozsa, J. M. Moss, D. R. Brown, and J. D. Bronson, *Phys. Rev.*

- Lett. **39**, 1188 (1977).
- [10] P. Chomaz and N. Frascaria, Phys. Rep. **252**, 275 (1995).
 - [11] T. Aumann, P. F. Bortignon, and H. Emling, Ann. Rev. Nucl. Part. Sci. **48**, 351 (1998).
 - [12] J.-A. Scarpaci, Nucl. Phys. **A731**, 175 (2004).
 - [13] C. Volpe, F. Catara, P. Chomaz, M. V. Andrés, and E. G. Lanza, Nucl. Phys. **A589**, 521 (1995).
 - [14] P. F. Bortignon and C. H. Dasso, Phys. Rev. C **56**, 574 (1997).
 - [15] M. Fallot, P. Chomaz, M. V. Andrés, F. Catara, E. G. Lanza, and J. A. Scarpaci, Nucl. Phys. **A729**, 699 (2003).
 - [16] C. Simenel and P. Chomaz, Phys. Rev. C **68**, 024302 (2003).
 - [17] P. Chomaz and C. Simenel, Nucl. Phys. **A731**, 188 (2004).
 - [18] E. G. Lanza, F. Catara, D. Gambacurta, M. V. Andrés, and P. Chomaz, Phys. Rev. C **79**, 054615 (2009).
 - [19] C. Simenel, P. Chomaz, and G. de France, Phys. Rev. Lett. **86**, 2971 (2001).
 - [20] C. Simenel, P. Chomaz, and G. de France, Phys. Rev. C **76**, 024609 (2007).
 - [21] P. Ring and P. Schuck, *The Nuclear Many-Body Problem* (Springer Verlag, Berlin, 1980).
 - [22] P. A. M. Dirac, Proc. Camb. Phil. Soc. **26**, 376 (1930).
 - [23] P. Chomaz, N. V. Giai, and S. Stringari, Phys. Lett. B **189**, 375 (1987).
 - [24] M. Gong, M. Tohyama and J. Randrup, Z. Phys. A **335**, 331 (1990).
 - [25] C. Y. Wong and H. H. K. Tang, Phys. Rev. Lett. **40**, 1070 (1978).
 - [26] D. Lacroix, P. Chomaz, and S. Ayik, Phys. Rev. C **58**, 2154 (1998).
 - [27] B. Avez, C. Simenel, and P. Chomaz, Phys. Rev. C **78**, 044318 (2008).
 - [28] S. Drożdż, S. Nishizaki, J. Speth, and J. Wambach, Physics Reports **197**, 1 (1990).
 - [29] D. Lacroix, A. Mai, P. von Neumann-Cosel, A. Richter, and J. Wambach, Phys. Lett. B **479**, 15 (2000).
 - [30] M. Tohyama, Phys. Rev. C **64**, 067304 (2001).
 - [31] M. Tohyama and A. S. Umar, Phys. Lett. B **549**, 72 (2002).
 - [32] S. J. Wang and W. Cassing, Ann. Phys. (N.Y.) **159**, 328 (1985).
 - [33] D. Lacroix, S. Ayik, and P. Chomaz, Phys. Rev. C **63**, 064305 (2001).
 - [34] D. Lacroix, S. Ayik, and P. Chomaz, Prog. in Part. and Nucl. Phys. **52**, 497 (2004).
 - [35] Y. M. Engel, Nucl. Phys. **A249**, 215 (1975).

- [36] P. Bonche, S. Koonin, and J. W. Negele, *Phys. Rev. C* **13**, 1226 (1976).
- [37] J. Blocki and H. Flocard, *Phys. Lett. B* **85**, 163 (1979).
- [38] A. S. Umar and V. E. Oberacker, *Phys. Rev. C* **71**, 034314 (2005).
- [39] J. A. Maruhn, P. G. Reinhard, P. D. Stevenson, J. R. Stone, and M. R. Strayer, *Phys. Rev. C* **71**, 064328 (2005).
- [40] T. Nakatsukasa and K. Yabana, *Phys. Rev. C* **71**, 024301 (2005).
- [41] C. Simenel, B. Avez, and D. Lacroix, in *Proceedings at the Joliot-Curie School, Maubuisson, 2007*, arXiv:0806.2714.
- [42] P. G. Reinhard, L. Guo, and J. A. Maruhn, *Eur. Phys. J. A* **32**, 19 (2007).
- [43] K.-H. Kim, T. Otsuka, and P. Bonche, *J. Phys. G* **23**, 1267 (1997).
- [44] E. Chabanat, P. Bonche, P. Haensel, J. Meyer, and R. Schaeffer, *Nucl. Phys.* **A635**, 231 (1998).
- [45] K. Bennaceur, P. Bonche, and J. Meyer, *C. R. Physique* **4**, 555 (2003).
- [46] P. Adrich *et al.*, *Phys. Rev. Lett.* **95**, 132501 (2005).
- [47] B. L. Berman and S. C. Fultz, *Rev. Mod. Phys.* **47**, 713 (1975).
- [48] M. M. Sharma, W. T. A. Borghols, S. Brandenburg, S. Crona, A. van der Woude, and M. N. Harakeh, *Phys. Rev. C* **38**, 2562 (1988).
- [49] P.-G. Reinhard, P. D. Stevenson, D. Almeded, J. A. Maruhn, and M. R. Strayer, *Phys. Rev. E* **73**, 036709 (2006).
- [50] E. Chabanat, P. Bonche, P. Haensel, J. Meyer, and R. Schaeffer, *Nucl. Phys.* **A627**, 710 (1997).
- [51] H. Steinwedel and J. H. D. Jensen, *Z. Naturforsch. A* **5**, 413 (1950).